

Assessing the effect of lens mass model in cosmological application with updated galaxy-scale strong gravitational lensing sample

Yun Chen¹, Ran Li^{1,2}, Yiping Shu^{3,4}

¹ Key Laboratory for Computational Astrophysics, National Astronomical Observatories, Chinese Academy of Sciences, Beijing, 100012, China;

² University of Chinese Academy of Sciences, 19 A Yuquan Rd, Shijingshan District, Beijing, 100049, China;

³ Purple Mountain Observatory, Chinese Academy of Sciences, 2 West Beijing Road, Nanjing 210008, China;

⁴ Institute of Astronomy, University of Cambridge, Madingley Road, Cambridge CB3 0HA, UK

22 April 2022

ABSTRACT

By comparing the dynamical mass and lensing mass of early type lens galaxies, one can constrain both the cosmological parameters and the density profiles of galaxies. In this paper, we explore the constraining power of this method on cosmological parameters, using a compiled sample of 157 galaxy-scale strong lensing systems, which is currently the largest sample with both high resolution imaging and stellar dynamical data. These selected lenses are all early-type galaxies with E or S0 morphologies and without significant substructures or close companion galaxies. We assume a power-law mass model for the lenses, and consider three different parameterizations for the slope (γ) of the total mass density profile ($\rho(r) \propto r^{-\gamma}$) to include the effect of the dependence of lens mass model on redshift and surface mass density. By fitting simultaneously the cosmological model and the lens mass model, we find that the cosmological parameters are not very well constrained with current data, and the posterior distribution on Ω_m is heavily dependent on the choice of parameterization for the lens mass model. By employing the Bayesian information criterion, we find the lens mass model including dependencies on both redshift and surface mass density is favored. We observe the dependencies of γ on the redshift and the surface mass density at $>3\sigma$ and $>5\sigma$ levels, respectively. We conclude that unless the significant dependencies of γ on both the redshift and the surface mass density are properly taken into account, the strong gravitational lensing systems under consideration cannot served as a kind of promising cosmological probes.

Key words: (cosmology:) cosmological parameters - cosmology: observations - gravitational lensing: strong - galaxies: structure

1 INTRODUCTION

In the last two decades, owing to the advent of powerful new space and ground-based telescopes for imaging and spectroscopic observations, many new strong gravitational lensing (SGL) systems have been discovered. Thus it has become achievable and significant to extract the information of lens objects and cosmological parameters from SGL data. Since the number of observed galaxy-scale SGL systems is much more than that of galaxy cluster-scale SGL systems, most statistical analyses have utilized the galaxy-scale SGL sample. In practice, several different quantities can be adopted as statistical quantities with galaxy-scale SGL sample, including the distribution of image angular separations (see, e.g., Turner et al. 1984; Dyer 1984; Chiba & Yoshii 1999; Dev et al. 2004; Cao & Zhu 2012), the distribution of lens redshifts (see, e.g., Turner et al. 1984; Kochanek 1992; Ofek et al. 2003; Mitchell et al. 2005; Cao et al. 2012a), the time delay between images ($\Delta\tau$) (see, e.g., Refsdal 1964; Treu & Marshall 2016; Bonvin et al. 2017), and the velocity dispersion (σ) of lenses (see, e.g., Futamase & Yoshida 2001; Biesiada 2006; Grillo et al. 2008; Schwab et al. 2010; Cao

et al. 2017). The major disadvantage of using the distributions of image angular separations and lens redshifts as statistical quantities is that the theoretically predicted values of these two are dependent not only on the lens mass model but also on the lens luminosity function. While the theoretical predictions of $\Delta\tau$ and σ are dependent only on the lens mass model but not on the luminosity function. Thus the methods of using $\Delta\tau$ and σ as statistical quantities are more popular at present. According to the theoretical analysis, one can see that $\Delta\tau$ is more sensitive to the cosmological parameters than σ (Paraficz & Hjorth 2009; Wei & Wu 2017). The fact also proves that the measurements of $\Delta\tau$ are very powerful at constraints on the cosmological parameters and especially sensitive to the Hubble constant H_0 (Bonvin et al. 2017; Suyu et al. 2017; Liao et al. 2017). However, the related cosmological application is mainly limited by the uncertainty in the lens modeling and the small number of lenses with measured time delays. In contrast, the number of lenses with measured σ are much larger. Although the measurements of σ are weak at confining the cosmological parameters (see, e.g., Biesiada 2006; Cao et al. 2012b; Wang & Xu

2013; Chen et al. 2015; Cao et al. 2015; An et al. 2016; Xia et al. 2017; Cui et al. 2017; Li et al. 2018a), they are useful for investigating the lens mass models if the priors on cosmological parameters are given (see, e.g., Koopmans et al. 2009; Sonnenfeld et al. 2013a; Cao et al. 2016; Holanda et al. 2017).

By combining the observations of SGL and stellar dynamics in elliptical galaxies, one can use the lens velocity dispersion (VD) as statistical quantity to put constraints on both the cosmological parameters and the density profiles of galaxies. The core idea of this method is that the gravitational mass M_{grl}^E and the dynamical mass M_{dyn}^E enclosed within the disk defined by the so-called Einstein ring should be equivalent, namely, $M_{\text{grl}}^E = M_{\text{dyn}}^E$. Further, M_{grl}^E inferring from the strong lensing data depends on cosmological parameters, and M_{dyn}^E inferring from the stellar VD depends on the lens mass model, so one can relate the VD with the model parameters including both cosmological and lens mass model parameters. This method can be traced back to Futamase & Yoshida (2001), but at that time there were no available observational data of lens VD. Grillo et al. (2008) first applied this method to constrain cosmological parameters with observational data, wherein the sample included 20 SGL systems from the Lens Structure and Dynamics (LSD) survey and the Sloan Lens ACS (SLACS) survey. In the literature, a recent compiled sample which can be used in this method includes 118 galaxy-scale SGL systems (Cao et al. 2015, hereafter C15) from the SLACS survey, the Baryon Oscillation Spectroscopic Survey (BOSS) emission-line lens survey (BELLS), the LSD survey, and the Strong Lensing Legacy Survey (SL2S). In this paper, we update the sample with definite criteria by taking advantage of new observational data, and then explore the effect of lens mass model on constraining cosmological parameters, as well as evaluate several different lens mass models.

The rest of the paper is organized as follows. In Section 2, we demonstrate the methodology of using the lens velocity dispersion as statistical quantity to constrain model parameters. Then, in Section 3 the SGL data sample used in our analysis is introduced. In Section 4, we first investigate the sensitivity of the sample under consideration to cosmological parameters, and diagnose whether our lens sample has any evolutionary signal via the qualitative and semi-quantitative analysis; and then carry out observational constraints on parameters of cosmology and lens mass models; and finally turn to compare several different lens mass models. In the last section, the main conclusions are summarized.

2 METHODOLOGY

As discussed in the last section, the method of using the galaxy lens VD as statistical quantity has some special merits. However, in this method, besides the imaging data of the SGL systems, one also has to possess the spectroscopic data of the systems and measure the central velocity dispersion of the lens galaxies from the spectroscopy. On the basis of various recent lensing surveys which have carried out both imaging and spectroscopic observations, this method has become feasible.

In this method, the main idea is that the projected gravitational mass M_{grl}^E and the projected dynamical mass M_{dyn}^E within the Einstein radius should be equivalent, i.e.,

$$M_{\text{grl}}^E = M_{\text{dyn}}^E. \quad (1)$$

From the theory of gravitational lensing, the projected gravitational mass within the Einstein radius is $M_{\text{grl}}^E = \Sigma_{\text{cr}} \pi R_E^2$. The Einstein radius R_E is determined by $R_E = \theta_E D_l$, wherein θ_E is the Einstein

angle, and D_l is the angular diameter distance between observer and lens. The critical surface mass density Σ_{cr} is defined by $\Sigma_{\text{cr}} = \frac{c^2}{4\pi G} \frac{D_s}{D_l D_{ls}}$, where D_{ls} is the angular diameter distance between lens and source, and D_s is that between observer and source. Thus, one can further figure out

$$M_{\text{grl}}^E = \frac{c^2}{4G} \frac{D_s D_l}{D_{ls}} \theta_E^2, \quad (2)$$

wherein the distances D_s , D_l and D_{ls} are dependent on the cosmological model.

To estimate the projected dynamical mass M_{dyn}^E from the lens galaxy VD, one must first suppose the mass distribution model for the lens galaxy. Here we choose a general mass model (Koopmans 2006) for the lens galaxies which are early-type galaxies (ETGs) with E or S0 morphologies:

$$\begin{cases} \rho(r) &= \rho_0 r^{-\gamma} \\ \nu(r) &= \nu_0 r^{-\delta} \\ \beta(r) &= 1 - \sigma_\theta^2 / \sigma_r^2 \end{cases} \quad (3)$$

where $\rho(r)$ is the total (i.e. luminous plus dark-matter) mass density distribution, and $\nu(r)$ is the luminosity density of stars. The parameter $\beta(r)$ denotes the anisotropy of the stellar velocity dispersion, and is also called as the stellar orbital anisotropy, where σ_θ and σ_r are the tangential and radial velocity dispersions, respectively. Based on the assumption that the relationship between stellar number density $n(r)$ and stellar luminosity density $\nu(r)$ is spatially constant, an assumption unlikely to be violated appreciably within the effective radius of the early-type lens galaxies under consideration, the radial Jeans equation in Spherical Coordinate can be written as

$$\frac{d}{dr}[\nu(r)\sigma_r^2] + \frac{2\beta}{r}\nu(r)\sigma_r^2 = -\nu(r)\frac{d\Phi}{dr}, \quad (4)$$

where

$$\frac{d\Phi}{dr} = \frac{GM(r)}{r^2}, \quad (5)$$

and $M(r)$ is the total mass inside a sphere with radius r . By substituting Eq. (5) into Eq. (4), one can get the expression for σ_r^2 ,

$$\sigma_r^2(r) = \frac{G \int_r^\infty dr' r'^{2\beta-2} \nu(r') M(r')}{r^{2\beta} \nu(r)}, \quad (6)$$

By defining r to be the spherical radial coordinate from the lens center, Z to be the axis along the line of sight (LOS), and R to be the cylindrical radius which is perpendicular to the LOS, then one has $r^2 = R^2 + Z^2$. The projected dynamical mass M_{dyn} contained within a cylinder of radius equal to the Einstein radius R_E can be calculated with

$$M_{\text{dyn}}^E = \int_0^{R_E} dR 2\pi R' \Sigma(R'), \quad (7)$$

where

$$\begin{aligned} \Sigma(R) &= \int_{-\infty}^{\infty} \rho(r) dZ \\ &= \int_{-\infty}^{\infty} dZ \frac{\rho_0}{r_0^{-\gamma}} (Z^2 + R^2)^{-\gamma/2} \\ &= \sqrt{\pi} R^{1-\gamma} \frac{\Gamma(\frac{\gamma-1}{2})}{\Gamma(\gamma/2)} \frac{\rho_0}{r_0^{-\gamma}} \end{aligned} \quad (8)$$

By substituting Eq.(8) into Eq.(7), one can have

$$M_{\text{dyn}}^E = 2\pi^{3/2} \frac{R_E^{3-\gamma}}{3-\gamma} \frac{\Gamma(\frac{\gamma-1}{2})}{\Gamma(\gamma/2)} \frac{\rho_0}{r_0^{-\gamma}}. \quad (9)$$

The total mass contained within a sphere with radius r is

$$M(r) = \int_0^r dr' 4\pi r'^2 \rho(r') = 4\pi \frac{\rho_0}{r_0^{-\gamma}} \frac{r^{3-\gamma}}{3-\gamma}. \quad (10)$$

By combining Eqs. (9) and (10), one can further have

$$M(r) = \frac{2}{\sqrt{\pi}} \frac{\Gamma(\gamma/2)}{\Gamma(\frac{\gamma-1}{2})} \left(\frac{r}{R_E}\right)^{3-\gamma} M_{\text{dyn}}^E. \quad (11)$$

By substituting Eqs. (11) and (3) into Eq. (6), one reads

$$\sigma_r^2(r) = \frac{2}{\sqrt{\pi}} \frac{GM_{\text{dyn}}^E}{R_E} \frac{1}{\xi - 2\beta} \frac{\Gamma(\gamma/2)}{\Gamma(\frac{\gamma-1}{2})} \left(\frac{r}{R_E}\right)^{2-\gamma}, \quad (12)$$

where $\xi = \gamma + \delta - 2$, and β is assumed to be independent of the radius r .

The actual velocity dispersion of the lens galaxy measured by the observation is the component of luminosity-weighted average along the LOS and over the effective spectroscopic aperture R_A , that can be expressed mathematically

$$\sigma_{\parallel}^2(\leq R_A) = \frac{\int_0^{R_A} dR 2\pi R \int_{-\infty}^{\infty} dZ \sigma_{\text{los}}^2 v(r)}{\int_0^{R_A} dR 2\pi R \int_{-\infty}^{\infty} dZ v(r)} \quad (13)$$

where σ_{los}^2 is the LOS velocity dispersion, which is a combination of the radial (σ_r^2) and tangential (σ_t^2) velocity dispersions. Using θ to indicate the angle between the LOS (Z-axis) and the radial direction (r-axis), then one reads

$$\begin{aligned} \sigma_{\text{los}}^2 &= (\sigma_r \cos \theta)^2 + (\sigma_t \sin \theta)^2 \\ &= \sigma_r^2 \frac{r^2 - R^2}{r^2} + \sigma_t^2 \frac{R^2}{r^2} \\ &= \sigma_r^2 \left(1 - \frac{R^2}{r^2}\right) + (1 - \beta) \sigma_r^2 \frac{R^2}{r^2} \\ &= \sigma_r^2 \left(1 - \beta \frac{R^2}{r^2}\right) \end{aligned} \quad (14)$$

By substituting Eq.(14) into Eq.(13), one can read

$$\sigma_{\parallel}^2(\leq R_A) = \frac{\int_0^{R_A} dR 2\pi R \int_{-\infty}^{\infty} dZ \sigma_r^2(r) (1 - \beta \frac{R^2}{r^2}) v(r)}{\int_0^{R_A} dR 2\pi R \int_{-\infty}^{\infty} dZ v(r)} \quad (15)$$

Further, by substituting Eq.(12) and (3) into Eq.(15), one obtains

$$\sigma_{\parallel}^2(\leq R_A) = \frac{2}{\sqrt{\pi}} \frac{GM_{\text{dyn}}^E}{R_E} \frac{3-\delta}{(\xi-2\beta)(3-\xi)} \left[\frac{\Gamma[(\xi-1)/2]}{\Gamma(\xi/2)} - \beta \frac{\Gamma[(\xi+1)/2]}{\Gamma[(\xi+2)/2]} \right] \frac{\Gamma(\gamma/2)\Gamma(\delta/2)}{\Gamma[(\gamma-1)/2]\Gamma[(\delta-1)/2]} \left(\frac{R_A}{R_E}\right)^{2-\gamma}. \quad (16)$$

Finally, with the relation expressed in Eq.(1), the above formula can be rewritten as

$$\sigma_{\parallel}^2(\leq R_A) = \frac{c^2}{2\sqrt{\pi}} \frac{D_s}{D_{ls}} \theta_E \frac{3-\delta}{(\xi-2\beta)(3-\xi)} \left[\frac{\Gamma[(\xi-1)/2]}{\Gamma(\xi/2)} - \beta \frac{\Gamma[(\xi+1)/2]}{\Gamma[(\xi+2)/2]} \right] \frac{\Gamma(\gamma/2)\Gamma(\delta/2)}{\Gamma[(\gamma-1)/2]\Gamma[(\delta-1)/2]} \left(\frac{\theta_A}{\theta_E}\right)^{2-\gamma}, \quad (17)$$

where $R_A = \theta_A D_l$.

From the spectroscopic data, one can measure the velocity dispersion σ_{ap} inside the circular aperture with the angular radius θ_{ap} . In practice, if the σ_{ap} are measured within rectangular apertures, one usually derives the equivalent circular apertures with the angular radii θ_{ap} following Jørgensen et al. (1995),

$$\theta_{\text{ap}} \approx 1.025 \times \sqrt{(\theta_x \theta_y / \pi)}, \quad (18)$$

where θ_x and θ_y are the angular sizes of width and length of the

rectangular aperture. More precisely, σ_{ap} is the projected, luminosity weighted average of the radially dependent velocity dispersion profile of the lensing galaxy inside θ_{ap} . For a fair comparison and in consideration of the effect of the aperture size on the measurements of velocity dispersions, all velocity dispersions σ_{ap} measured within apertures of arbitrary sizes, are normalized to a typical physical aperture, σ_{e2} , with the radius $R_{\text{eff}}/2$, where R_{eff} is the half-light radius of the lens galaxy, and $R_{\text{eff}}/2$ is a quantity that is well-matched to the typical Einstein radius. Following the prescription, one can use the aperture correction formula,

$$\sigma_{\parallel}^{\text{obs}} \equiv \sigma_{e2} = \sigma_{\text{ap}} [\theta_{\text{eff}} / (2\theta_{\text{ap}})]^{\eta}, \quad (19)$$

where $\theta_{\text{eff}} = R_{\text{eff}}/D_l$. The best-fitting values of the correction factor η are different when using different observational samples. For example, the best-fitting values of η are -0.04 , -0.06 and -0.066 ± 0.035 found by Jørgensen et al. (1995), Mehlert et al. (2003) and Cappellari et al. (2006), respectively. Compared with the values of σ_{e2} calculated with $\eta = -0.04$, the relative differences of σ_{e2} in the cases of $\eta = -0.06$ and $\eta = -0.066$ are smaller than 5% for the lenses under consideration. In practice, we first calculate the mean value and the statistical error of σ_{e2} with $\eta = -0.04$ following Jørgensen et al. (1995), where the statistical error, $\Delta\sigma_{e2}^{\text{stat}}$, is propagated from the measurement error of σ_{ap} . And on this basis, we conservatively assume an uncertainty of 5% on σ_{e2} due to the aperture correction, which is marked as $\Delta\sigma_{e2}^{\text{AC}}$.

In order to compare the observational values of the VD with the corresponding model-predicted ones, one needs to calculate the theoretical value of the VD within the radius $R_{\text{eff}}/2$ from Eq. (17),

$$\sigma_{\parallel}(\leq \theta_{\text{eff}}/2) = \sqrt{\frac{c^2}{2\sqrt{\pi}} \frac{D_s}{D_{ls}} \theta_E \frac{3-\delta}{(\xi-2\beta)(3-\xi)} F(\gamma, \delta, \beta) \left(\frac{\theta_{\text{eff}}}{2\theta_E}\right)^{(2-\gamma)}}, \quad (20)$$

where

$$F = \left[\frac{\Gamma[(\xi-1)/2]}{\Gamma(\xi/2)} - \beta \frac{\Gamma[(\xi+1)/2]}{\Gamma[(\xi+2)/2]} \right] \frac{\Gamma(\gamma/2)\Gamma(\delta/2)}{\Gamma[(\gamma-1)/2]\Gamma[(\delta-1)/2]}. \quad (21)$$

In the case of $\gamma = \delta = 2$ and $\beta = 0$, the mass model is reduced to the well-known Singular Isothermal Sphere (SIS) model, and the predicted value of the VD is recovered to

$$\sigma_{\text{SIS}} = \sqrt{\frac{c^2}{4\pi} \frac{D_s}{D_{ls}} \theta_E}. \quad (22)$$

In our analysis, the likelihood is assumed to be

$$\mathcal{L} \propto e^{-\chi^2/2}. \quad (23)$$

χ^2 is constructed as

$$\chi^2 = \sum_{i=1}^N \left(\frac{\sigma_{\parallel,i}^{\text{th}} - \sigma_{\parallel,i}^{\text{obs}}}{\Delta\sigma_{\parallel,i}^{\text{obs}}} \right)^2, \quad (24)$$

where N is the number of the data points, $\Delta\sigma_{\parallel,i}^{\text{obs}}$ is the observational error of $\sigma_{\parallel,i}^{\text{obs}}$, which is calculated with $(\Delta\sigma_{\parallel,i}^{\text{obs}})^2 = (\Delta\sigma_{e2}^{\text{stat}})^2 + (\Delta\sigma_{e2}^{\text{AC}})^2$. One can obtain $\sigma_{\parallel,i}^{\text{obs}}$ and $\sigma_{\parallel,i}^{\text{th}}$ from Eqs. (19) and (20), respectively.

3 DATA SAMPLE

According to the analysis in the last section, one can learn that the method under consideration requires the following information from observations, including the lens redshift z_l , the source redshift

z_s , the Einstein angle θ_E , the central VD of the lens galaxy σ_{ap} , the spectroscopic aperture angular radius θ_{ap} , and the half-light angular radius of the lens galaxy θ_{eff} . Additionally, to ensure the validity of the assumption of spherical symmetry on the lens galaxy, the selected lens galaxies should satisfy the following conditions: (i) the lens galaxy should be ETGs with E or S0 morphologies; and (ii) the lens galaxy should not have significant substructure or close massive companion. Some lens galaxies from C15 do not satisfy the condition (i). Here we assemble a sample including 157 definite galaxy-scale SGL systems which meet all the requirements mentioned above, where 5 systems from the LSD survey¹ (Koopmans & Treu 2002; Treu & Koopmans 2002; Koopmans & Treu 2003; Treu & Koopmans 2004), 26 from the SL2S (Ruff et al. 2011; Sonnenfeld et al. 2013a,b; Sonnenfeld et al. 2015), 53 from the SLACS (Bolton et al. 2008; Auger et al. 2009, 2010), 38 from the an extension of the SLACS survey known as “SLACS for the Masses” (hereafter S4TM, Shu et al. 2015; Shu et al. 2017), 21 from the BELLS (Brownstein et al. 2012), and 14 from the BELLS for GALaxy-Ly α Emitter sYstemsGALLERY (hereafter BELLS GALLERY, Shu et al. 2016a,b). The useful information of these 157 systems is listed in Table 1.

The velocity dispersions of the lenses from LSD and SL2S surveys, which are measured within rectangular slits, are transformed into velocity dispersions σ_{e2} , within a circular aperture with radius $R_{eff}/2$ based on Eqs.(18) and (19). The SLACS and S4TM surveys select candidates from Sloan Digital Sky Survey I (SDSS-I, Eisenstein et al. 2001; Strauss et al. 2002) data, in which the velocity dispersions of the lenses are measured within the $1.5''$ -radius fibers. The lens candidates of the BELLS and BELLS GALLERY surveys are spectroscopically selected from the BOSS (Dawson et al. 2013) of the Sloan Digital Sky Survey-III (SDSS-III, Eisenstein et al. 2011), in which the VD of the lenses are measured within the $1''$ -radius fibers. These velocity dispersions measured with fibers are corrected to σ_{e2} based on Eq.(19). The distribution of the whole SGL sample is shown in Fig. 1. From the upper panels of Fig. 1, one can see that $\sim 30\%$ of the lenses are located at $z_l \sim 0.2$, and only $\sim 5\%$ located at $z_l > 0.75$. The lower panels of Fig. 1 show that $\sim 80\%$ of the lenses possess the velocity dispersions $180 \text{ km s}^{-1} < \sigma_{e2} < 300 \text{ km s}^{-1}$.

4 ANALYSIS AND RESULTS

4.1 Qualitative analysis

4.1.1 Sensitivity to cosmological parameters

From Eq. (20) one can see that the cosmological model enters into the theoretical observable $\sigma_{||}^{\text{th}}$ not through a distance measure directly, but rather through a distance ratio

$$\frac{D_s}{D_{ls}} = \frac{\int_0^{z_s} \frac{dz}{E(z; \mathbf{p})}}{\int_{z_l}^{z_s} \frac{dz}{E(z; \mathbf{p})}}, \quad (25)$$

where in the framework of the flat FLRW metric the theoretical values of D_s and D_{ls} can be obtained by

$$D_s(z_s; \mathbf{p}, H_0) = \frac{c}{H_0(1+z_s)} \int_0^{z_s} \frac{dz}{E(z; \mathbf{p})}, \quad (26)$$

and

$$D_{ls}(z_l, z_s; \mathbf{p}, H_0) = \frac{c}{H_0(1+z_s)} \int_{z_l}^{z_s} \frac{dz}{E(z; \mathbf{p})}, \quad (27)$$

respectively, where \mathbf{p} denotes the parameter space of the considered cosmological model, and $E = H/H_0$ is the dimensionless Hubble parameter, and c is the velocity of light. Hence, the advantage and disadvantage are both remarkable in this method. The positive side is that theoretical observable is independent of the Hubble constant H_0 which gets canceled in the distance ratio. Currently, the trouble with H_0 is that the values measured by different methods are significantly in tension (see, e.g., Bernal et al. 2016; Chen et al. 2017; Freedman 2017). The most representative example is that the indirect (model-dependent) measurement of H_0 from Planck mission (Planck Collaboration: Ade, P. A. R., et al. 2014, 2016) when Λ CDM model is assumed is much smaller than and in tension (at $> 2\sigma$ confidence level) with the direct measurement from Hubble Space Telescope (HST) key project (Riess et al. 2011, 2016). Thus, it is a very tough problem to set a prior on H_0 . In this situation, the significant advantage of the method under consideration is that it directly avoids the effect of H_0 .

On the other side, the main disadvantage is that the power of estimating cosmological parameters is poor. The distance ratio D_s/D_{ls} is a ratio of two integrals which have the same integrand (i.e., $1/E(z; \mathbf{p})$) and differ only by the limits of integration, so the theoretical observable $\sigma_{||}^{\text{th}} \propto \sqrt{D_s/D_{ls}}$ is insensitive to the cosmological parameters involved in the integrand (Biesiada et al. 2010). In Fig. 2, we show the impact of the matter-density parameter Ω_m on the distance ratio by taking a spatially flat Λ CDM model with $\Omega_m = 0.3$ as a fiducial cosmological model. The three panels of Fig. 2 display the evolution of D_s/D_{ls} with respect to the source redshift z_s along with variety of Ω_m , corresponding to the cases of the lens redshift $z_l = 0.1, 0.5$, and 1 from left to right. The general trend is that the sensitivity of D_s/D_{ls} to Ω_m increases with the increase of z_l . In Fig. 2, the shadows denote the cases that the relative uncertainties of D_s/D_{ls} are 10% and 20%, respectively, with respect to the fiducial value. One can see that an individual lens with $z_l = 0.1$ cannot put any constraint on Ω_m even when D_s/D_{ls} only has 10% uncertainty. An individual lens with $z_l = 0.5$ can bound on Ω_m with $\sim 80\%$ – 160% relative uncertainty when D_s/D_{ls} only has 10% uncertainty, but cannot put any constraint on Ω_m when the uncertainty of D_s/D_{ls} increases to 20%. Unfortunately, with regard to the SGL sample under consideration, the typical values of the relative uncertainties of D_s/D_{ls} ² are approximately 10% and 20% at $z_l \approx 0.1$ and 0.5 , respectively. It means that most lenses with $z_l < 0.5$ in our sample do not contribute to the limit on Ω_m . An individual lens with $z_l = 1$ can put a limit on Ω_m with $\sim 50\%$ – 100% ($\sim 80\%$ – 200%) relative uncertainty, corresponding to D_s/D_{ls} with 10%(20%) uncertainty. In our sample, there is only one system with $z_l > 1$, that is MG2016+112 with $z_l = 1.004$ from LSD survey. In general, one is not able to make a reliable estimate on Ω_m with the sample under consideration. After repeating similar analyses for other cosmological parameters (i.e., the equation of state parameter of dark energy, and the curvature parameter), we find out that the current sample is really weak at confining these cosmological parameters.

² The uncertainty on D_s/D_{ls} is mainly propagated from that on σ_{e2} . The relative uncertainty on D_s/D_{ls} is about 2 times of that on σ_{e2} because of $D_s/D_{ls} \propto \sigma_{e2}^2$.

¹ <http://web.physics.ucsb.edu/~tt/LSD/>

4.1.2 Diagnosing the evolution of the lens sample's mass-density profile

In order to diagnose whether there is any evolutionary signal among our lens sample, we divide the entire sample into several different sub-samples, and then check whether significant differences exist among the ranges of lens mass model parameters constrained from different sub-samples. In practice, we divide the entire sample into four sub-samples according to the velocity dispersion: $\sigma_{e2} \leq 210$ ($n = 40$), $210 < \sigma_{e2} \leq 243$ ($n = 39$), $243 < \sigma_{e2} \leq 276$ ($n = 39$), and $\sigma_{e2} > 276$ ($n = 39$), where σ_{e2} is in unit of km/s, and n is the size of each sub-sample. Note that the breakpoints are chosen to insure that the sub-sample sizes are nearly equal.

We carry out observational constraints on all parameters of the lens mass model formulized by Eq. (3) from four sub-samples, respectively, by keeping the cosmological parameters fixed with $\Omega_m = 0.3$ in the framework of a spatially flat Λ CDM model. In our analysis, the likelihood is computed with Eqs. (23) and (24). We derive the posterior probability distributions of parameters through an affine-invariant Markov chain Monte Carlo (MCMC) Ensemble sampler (emcee; Foreman-Mackey et al. 2013). The one-dimensional (1D) probability distributions and two-dimensional (2D) contours for the model parameters are displayed in Fig. 3. It turns out that the limits on parameter γ from different sub-samples have significant distinctions. While the ranges of δ and β obtained from different sub-samples are consistent at 68% confidence level. In addition, the limits on these two parameters are much weaker than those on γ . It is reasonable because, theoretically, the deflection of light due to gravitational lensing is more sensitive to the total mass, so the lensing data are most sensitive to the parameter γ . In general, the parameter γ presents the most significant evolutionary signal. In other words, the dependence of γ on the properties of lenses should not be ignored in the statistical analysis.

4.2 Observational constraints

4.2.1 Constraints on parameters of cosmology and lens mass models

We assume a kind of spherically symmetric mass distributions (i.e. Eq. (3)) for the lens galaxies in the kinematic analysis. As discussed above, the dependence of γ on the properties of lenses should be taken into account. In the literature, the dependence of γ on the redshift has been widely studied (see, e.g., Ruff et al. 2011; Bolton et al. 2012; Cao et al. 2015; Cao et al. 2016; Cui et al. 2017; Holanda et al. 2017). Besides, Auger et al. (2010) also found a significant correlation between γ and total mass surface density, that has also been confirmed by Dutton & Treu (2014) and Sonnenfeld et al. (2013a). In the light of these works, we specifically consider three lens mass models on the basis of Eq. (3), corresponding to three parameterizations for γ , namely:

- $P_1 : \gamma = \text{Constant}$,
- $P_2 : \gamma = \gamma_0 + \gamma_z * z_l$,
- $P_3 : \gamma = \gamma_0 + \gamma_z * z_l + \gamma_s * \log \tilde{\Sigma}$,

where γ is treated as an arbitrary constant in case P_1 , and its dependence on the lens redshift z_l is considered in case P_2 . Besides, the dependence on both the redshift and the surface mass density is taken into account in case P_3 . According to the virial theorem, the projected dynamical mass within the radius $R_{\text{eff}}/2$ satisfies $M_{e2}^{\text{dyn}} \propto \sigma_{e2}^2 R_{\text{eff}}$ (see, e.g., Auger et al. 2010), so the corresponding surface mass density is $\Sigma \propto \sigma_{e2}^2 / R_{\text{eff}}$. Here, we use $\tilde{\Sigma}$ to denote

the normalized surface mass density of the lens galaxy, which is expressed as

$$\tilde{\Sigma} = \frac{(\sigma_{e2}/100 \text{ km s}^{-1})^2}{R_{\text{eff}}/10 h^{-1} \text{ kpc}}, \quad (28)$$

where the usual convention of writing the Hubble constant as $H_0 = 100h \text{ km s}^{-1} \text{ Mpc}^{-1}$ is adopted. Hereafter, “Model 1”, “Model 2”, and “Model 3” denote the lens mass models in which γ is parameterized in the forms of P_1 , P_2 , and P_3 , respectively.

As mentioned above, the sample under consideration is quit weak at constraining cosmological parameters, so constraining too many cosmological parameters simultaneously would only distort the results. Thus, we only attempt to fit Ω_m in the framework of flat Λ CDM model, where Ω_m is the only free parameter of cosmology. We then conduct observational constraints on Ω_m and lens mass model parameters in the schemes of “Model 1”, “Model 2” and “Model 3”, respectively. The results are displayed in Figure 4, including the 1D probability distributions and 2D contours for the parameters of interest. The limits on Ω_m at 68% (95%) confidence level are $\Omega_m < 0.047$ ($\Omega_m < 0.113$), $\Omega_m < 0.159$ ($\Omega_m < 0.401$) and $0.432 < \Omega_m < 0.808$ ($0.261 < \Omega_m < 0.948$) in the frameworks of three different lens mass models, respectively. The main tendencies can be summarized to three aspects. First, the limits on Ω_m are significantly dependent on the lens mass model. The allowed range of Ω_m in the third scenario is inconsistent with those obtained in the former two at 68% confidence level. Second, the constraints on Ω_m are weak. In the first two scenarios, the lower limits on Ω_m are unavailable. In the last scenario, the relative uncertainty of Ω_m is about 30% at 68% confidence level. It is consistent with the qualitative analysis mentioned previously, which reveals that the sample under consideration is insensitivity to Ω_m . Third, the estimations on Ω_m are biased. The mean value of Ω_m constrained from the standard cosmological probes is around 0.3 (see, e.g. Huterer & Shafer 2018; Scolnic et al. 2018; Alam et al. 2017), such as $\Omega_m = 0.315 \pm 0.007$ in the framework of flat Λ CDM model obtained from the recent Planck 2018 result (Planck Collaboration: Aghanim, N., et al. 2018). In the first scenario, the limit on Ω_m is inconsistent with that from the Planck result at 95% confidence level, and the allowed values of Ω_m are especially low. In the second scenario, it is consistent with the Planck result at 95% confidence level, but the mean value of Ω_m is much lower. In the last scenario, it is consistent with the Planck result at 95% confidence level, but the mean value is much higher. The bias in the estimation of Ω_m must be related to the insensitivity of the distance ratio D_s/D_{ls} to the cosmological parameters as discussed previously. Besides, it may also be due to some unknown systematic errors.

This is the first time to constrain the cosmological parameter in the scenario of considering the dependence of γ on both redshift and surface mass density. In C15, they constrained the equation of state (EoS) of dark energy (with other cosmological parameters fixed) from their sample with 118 systems in the scenarios of P_1 and P_2 . From the results listed in Table 2 of C15, one can see that the constraints on the EoS of dark energy are also quit weak, the uncertainties are bigger than 30%.

4.2.2 Comparing lens mass models

As discussed previously, one is not able to make reliable estimates for cosmological parameters based on the current lensing and kinematics data of the galaxy-scale lens sample. What is more, the limits on cosmological parameters are quite dependent on the lens mass model. So it is necessary to compare the lens mass models and

select the most competitive one, that can supply helpful reference for future studies on selecting the lens mass model. And fortunately, the key cosmological parameters have been determined precisely by the current standard cosmological probes. Given these things, we choose to compare the lens mass models by using priors on cosmological parameters from the Planck 2018 results (Planck Collaboration: Aghanim, N., et al. 2018), i.e., assuming a flat Λ CDM model with $\Omega_m = 0.315 \pm 0.007$ as a fiducial cosmological model. Then, we put observational constraints on the lens mass models. Our results are summarized in Table 2 and Figure 5. The 1D probability distributions and 2D contours for the parameters of interest are shown in Figure 5. The mean values with 68% confidence limits for the parameters listed in Table 2 are derived from the corresponding 1D marginalized distribution probabilities.

In the framework of “Model 1” (i.e., $\gamma = \text{Const.}$), one can find out that the limit on γ is much tighter than those on δ and β , where the relative uncertainties of γ , δ and β are $\sim 2\%$, $\sim 25\%$ and $\sim 100\%$, respectively. It agrees with the theory of gravitational lensing (see, e.g., Wambsganss 1998), which indicates that the lensing data are most sensitive to the parameter γ as mentioned previously. Comparing with the result in the “Model 1”, we observe a minor shift in the mean value and a significant reduction in the uncertainty for δ in the other two models. More specifically, the relative uncertainty of δ is $\sim 25\%$ in the “Model 1”, which is reduced to $\sim 15\%$ in the “Model 2”, and further to $\sim 5\%$ in the “Model 3”. In contrast, there is a significant shift in the mean value of β , but because of the large uncertainty on it, the limits on β are consistent at 68% confidence level in all three scenarios. And, the mean value of β in “Model 3” is much closer to that from Koopmans et al. (2009). In the framework of “Model 2”, $\gamma_z = 0$ is ruled out at $\sim 2.3\sigma$ level. Cao et al. (2016) used the sample of C15 to constrain the lens mass model parameters in the case of “Model 2” with cosmological parameters fixed, but without considering the dependence of γ on surface density. Thus, we just can compare our result with theirs in the case of “Model 2”. While they found the dependence on redshift at $\sim 1.5\sigma$ level from C15’s sample. It turns out that the dependence of γ on the redshift can be observed at higher confidence level based on our updated sample. Further, in the framework of “Model 3”, $\gamma_z = 0$ is ruled out at $\sim 3.5\sigma$ level, and $\gamma_s = 0$ is ruled out at $\sim 6\sigma$ level. Sonnenfeld et al. (2013a) found the dependence of γ on redshift and surface mass density at $\sim 3.1\sigma$ and $\sim 5.4\sigma$ levels, respectively, from the SL2S, SLACS and LSD lenses. It implies that the corresponding signals are extracted from our sample at a bit higher levels. Based on the previous analysis, we conclude that dependencies of γ on both the redshift and the surface mass density are very significant.

Furthermore, we employ the Bayesian information criterion (BIC) to compare the three models. The BIC (Schwarz 1978) is defined as

$$\text{BIC} = -2 \ln \mathcal{L}_{\max} + k \ln N, \quad (29)$$

where \mathcal{L}_{\max} is the maximum likelihood (satisfying $-2 \ln \mathcal{L}_{\max} = \chi^2_{\min}$ under the Gaussian assumption), k is the number of the parameters of the considered model, and N is the number of data points used in the fitting. The BIC is widely used in a cosmological context (see, e.g., Liddle 2004; Godłowski & Szydlowski 2005; Magueijo & Sorkin 2007; Mukherjee et al. 2006; Biesiada 2007; Davis et al. 2007; Li et al. 2013; Wen et al. 2018). This statistic prefers models that give a good fit with fewer parameters. The favorite model is the one with the minimum BIC value. The BIC values for the three models are 344.924, 334.259, and 194.804, respec-

tively. So, the most competitive one is “Model 3”, that is consistent with the previous conclusion.

In order to verify the robustness of the above conclusion, we then turn to consider the impacts of the prior on Ω_m and the systematic error in the velocity dispersion. In previous analyses, we have adopted a prior value on Ω_m from the Planck 2018 result. When changing the prior value to $\Omega_m = 0.308 \pm 0.012$ from the Planck 2015 result (Planck Collaboration: Ade et al. 2016), we find that the relative differences in the mean values of the lens model parameters are less than 3%, which brings in an insignificant impact on our conclusion. In addition, the systematic error in the velocity dispersion has not yet been taken into account. While Jiang & Kochanek (2007) considered five sources of systematic error in the velocity dispersion and found that the fractional systematic error is approximately 8%. When combining the 8% systematic error with the observational error in quadrature, we still can observe the dependence of γ on the redshift and the surface mass density at $\sim 3\sigma$ and $\sim 5\sigma$ levels, respectively.

5 SUMMARY AND CONCLUSIONS

We have compiled a galaxy-scale strong gravitational lensing sample including 157 systems with the gravitational lensing and stellar velocity dispersion measurements, which are selected with strict criteria to satisfy the assumption of spherical symmetry on the lens mass model. Actually, the selected lenses are all early-type galaxies with E or S0 morphologies. A kind of spherically symmetric mass distributions formulized by Eq.(3) is assumed for the lens galaxies throughout this paper. After carrying out the qualitative and semi-quantitative analysis, we find that the current sample is weak at confining cosmological parameters, and the lens mass model parameter γ (i.e., the slope of the total mass density profile) presents a significant evolutionary signal. Given this, we specifically consider three lens mass models on the basis of Eq. (3), corresponding to three parameterizations for the slope γ . The slope γ is treated as an arbitrary constant without considering any dependency in the first scenario (namely “Model 1”). And its dependence on the lens redshift is considered in the second scenario (namely “Model 2”). Further, its dependencies on both the redshift and the surface mass density of the lens are taken into account in the last scenario (namely “Model 3”). We first try to constrain both the cosmological and lens mass model parameters. However, it turns out that the limit on the cosmological parameter, Ω_m , is quit weak and biased, as well as quite dependent on the lens mass model. So, we turn to compare and select the lens mass models by keeping the cosmological parameters fixed. The result shows that the “Model 3” is most preferred by the current sample, and the dependencies of γ on the redshift and on the surface mass density are observed at $>3\sigma$ and $>5\sigma$ levels, respectively. And, as discussed in Sec. 4.2.2, the corresponding signals are observed at higher levels from our updated sample, compared to the previous studies. The consequence still holds after considering the impacts of the prior on Ω_m and the systematics error in the velocity dispersion. In addition, we have treated both the slope (δ) of the luminous matter density profile ($\nu(r) \propto r^{-\delta}$) and the orbit anisotropy parameter β as arbitrary constants in our observational constraints. However, Xu et al. (2017) found the dependencies of δ and β on stellar velocity dispersion and redshift at different confidence levels, based on the Illustris simulation. Even so, our results are still not in conflict with theirs, because the uncertainties on these two parameters obtained from our constraints can mimic the intrinsic spreads in these quantities.

Consequently, the dependencies of γ on both the redshift and the surface mass density are very significant, that should be taken into account in the cases of employing the strong gravitational lensing systems as cosmological probes. Moreover, the slope γ has a positive correlation with the surface mass density, and a negative correlation with the redshift. It is worth noting that the dependency of γ on redshift and surface mass density does not represent that the ETGs change their mass density profile over the lifetime (Sonnensfeld et al. 2013a), that mainly denotes the statistical feature of the population included in our sample. The overall trends show that, at a given redshift, the galaxies with high density also have steeper slopes; and, at fixed surface mass density, the galaxies at a lower redshift have steeper slopes. These trends are consistent with those obtained in the previous studies (e.g., Auger et al. 2010; Ruff et al. 2011; Bolton et al. 2012; Holanda et al. 2017; Sonnensfeld et al. 2013a; Li et al. 2018b). Understanding the deep meanings of these trends on the evolution of individual ETGs requires more other observational data, that is beyond the scope of this paper. Finally, we point out that besides the dependence of γ on redshift and surface mass density considered in this work, other important dependencies may also be found in future, that can lead to a more accurate phenomenological model for lens galaxies.

In addition, although the measurements of the velocity dispersions (σ) of lens galaxies alone are insufficient to make reliable estimates on the cosmological parameters, measurements of time delays ($\Delta\tau$) and the joint measurements of the former two ($\Delta\tau/\sigma^2$) are both proved to be more sensitive to the cosmological parameters (Paraficz & Hjorth 2009; Wei & Wu 2017). At present, the cosmological implementation is limited by the uncertainty in the lens modeling and the small number of lenses with measured time delays. One can anticipate significant improvements in these two aspects in view of the future observational facilities and hydrodynamic simulations of galaxy formation (see, e.g., Oguri & Marshall 2010; Suyu et al. 2017; Shu et al. 2018; Treu et al. 2018).

ACKNOWLEDGMENTS

We would like to thank Shuo Cao, Marek Biesiada, Lixin Xu, Guojian Wang, Qiao Wang, Ming Li, Jie Wang and Liang Gao for helpful discussions. YC has been supported by the National Natural Science Foundation of China (Nos. 11703034 and 11573031), and the NAOC Nebula Talents Program. RL has been supported by the National Key Program for Science and Technology Research and Development of China (2017YFB0203300), the National Natural Science Foundation of China (Nos. 11773032 and 118513), and the NAOC Nebula Talents Program. YS has been supported by the National Natural Science Foundation of China (Nos. 11603032 and 11333008), the 973 program (No. 2015CB857003), and the Royal Society – K.C. Wong International Fellowship (NF170995).

REFERENCES

- Alam, S., et al., 2017, *MNRAS*, 470, 2617.
 An, J., Chang, B.-R., & Xu, L.-X., 2016, *ChPhL*, 33, 9801
 Auger, M. W., et al., 2009, *ApJ*, 705, 1099.
 Auger, M. W., et al., 2010, *ApJ*, 724, 511.
 Bernal, J. L., Verde, L., & Riess, A. G., 2016, *JCAP*, 10, 019.
 Biesiada, M. 2006, *PhRvD*, 73, 3006.
 Biesiada, M. 2007, *JCAP*, 2, 3.
 Biesiada, M., Piorkowska, A., & Malec, B., 2010, *MNRAS*, 406, 1055.
 Bolton, A. S., et al., 2008, *ApJ*, 682, 964.
 Bolton, A. S., et al., 2012, *ApJ*, 757, 82.
 Bonvin, V., et al., 2017, *MNRAS*, 465, 4914
 Brownstein, J. R., et al., 2012, *ApJ*, 744, 41.
 Cao, S., Covone, G., & Zhu, Z.-H., 2012a, *ApJ*, 755 (2012) 31.
 Cao, S., et al., 2012b, *JCAP*, 03, 016.
 Cao, S. & Zhu, Z.-H., 2012, *A&A*, 538, 43.
 Cao, S., et al., 2015, *ApJ*, 806, 185 (C15)
 Cao, S., et al., 2016, *MNRAS*, 461, 2192.
 Cao, S., et al., 2017, *ApJ*, 835, 92.
 Cappellari, M., et al., 2006, *MNRAS*, 366, 1126
 Chen, Y., et al., 2015, *JCAP*, 02, 010.
 Chen, Y., Kumar, S., & Ratra, B., 2017, *ApJ*, 835, 86.
 Chiba, M., & Yoshii, Y., 1999, *ApJ*, 510, 42.
 Cui, J.-L., Li, H.-L. & Zhang, X., 2017, *Sci. China-Phys. Mech. Astron.*, 60, 080411.
 Davis, T. M., et al., 2007, *ApJ*, 666, 716.
 Dawson, K. S., et al., 2013, *AJ*, 145, 10.
 Dev, A., Jain, D., & Mahajan, S., 2004, *IJMPD*, 13, 1005.
 Dutton, A. A. & Treu, T., 2014, *MNRAS*, 438, 3594.
 Dyer, C. C., 1984, *ApJ*, 287, 26.
 Eisenstein, D. J., et al., 2001, *AJ*, 122, 2267.
 Eisenstein, D. J., et al., 2011, *AJ*, 142, 72.
 Foreman-Mackey, D., Hogg, D. W., Lang, D., & Goodman, J., 2013, *PASP*, 125, 306.
 Freedman, W. L., 2017, *Nature Astronomy*, 1, 0169.
 Futamase, T., & Yoshida, S., 2001, *PTHPh*, 105, 887.
 Godłowski, W., & Szydlowski, M. 2005, *Physics Letters B*, 623, 10.
 Grillo, C., Lombardi, M., & Bertin, G., 2008, *A&A*, 477, 397.
 Holanda, R. F. L., Pereira, S. H., & Jain, D., 2017, *MNRAS*, 471, 3079
 Huterer, D., & Shafer, D. L., 2018, *Reports on Progress in Physics*, 81, 016901.
 Jiang, G. & Kochanek, C. S., 2007, *ApJ*, 671, 1568.
 Jørgensen, I., Franx, M., & Kjaergaard, P., 1995, *MNRAS*, 276, 1341.
 Kochanek, C. S., 1992, *ApJ*, 384, 1.
 Koopmans, L. V. E. & Treu, T., 2002, *ApJ*, 568, L5.
 Koopmans, L. V. E. & Treu, T., 2003, *ApJ*, 583, 606.
 Koopmans, L. V. E., 2006, *EAS Publications Series*, 20, 161.
 Koopmans, L. V. E., et al., 2009, *ApJ*, 703, L51.
 Li, M., Li, X.-D., Wang, S., & Wang, Yi, 2013, *Frontiers of Physics*, 8, 828.
 Li, Z., et al., 2018a, *ApJ*, 854, 146.
 Li, R., Shu, Y., & Wang, J., 2018b, *MNRAS*, 480, 431.
 Liao, K., et al., 2017, *Nature Communications*, 8, 1148.
 Liddle, A. R., 2004, *MNRAS*, 351, L49.
 Magueijo, J., & Sorkin, R. D. 2007, *MNRAS*, 377, L39.
 Mehlert, D., Thomas, D., Saglia, R.P., Bender, R. & Wegner, G. 2003, *A&A*, 407, 423.
 Mitchell, J. L., et al., 2005, *ApJ*, 622, 81.
 Mukherjee, P., Parkinson, D., Corasaniti, P. S., Liddle, A. R., & Kunz, M. 2006, *MNRAS*, 369, 1725.
 Ofek, E. O., Rix, H.-W., & Maoz, D., 2003, *MNRAS*, 343, 639.
 Oguri, M., & Marshall, P. J., 2018, *MNRAS*, 405, 2579.
 Paraficz, D. & Hjorth J., 2009, *A&A*, 507, L49
 Planck Collaboration, Ade, P. A. R., et al., 2014, *A&A*, 571, A16.
 Planck Collaboration: Ade, P. A. R., et al., 2016, *A&A*, 594, A13.

- Planck Collaboration: Aghanim, N., et al, 2018, preprint, (arXiv:1807.06209).
- Refsdal, S., 1964, MNRAS, 128, 307.
- Riess, A. G., et al., 2011, ApJ, 730, 119.
- Riess, A. G., et al., 2016, ApJ, 826, 56.
- Ruff, A. J., et al., 2011, ApJ, 727, 96.
- Schwarz, G., 1978, The Annals of Statistics, 6, 461.
- Schwab, J., Bolton, A. S. & Rappaport, S. A., 2010, ApJ, 708, 750.
- Scolnic, D. M., et al., 2018, ApJ, 859, 101.
- Shu, Y., et al., 2015, ApJ, 803, 71.
- Shu, Y., et al., 2016a, ApJ, 824, 86.
- Shu, Y., et al., 2016b, ApJ, 833, 264.
- Shu, Y., et al., et al., 2017, ApJ, 851, 48.
- Shu, Y., et al., 2018, preprint, (arXiv:1803.07569)
- Sonnenfeld, A., et al., 2013a, ApJ, 777, 98.
- Sonnenfeld, A., Gavazzi, R., Suyu, S. H., Treu, T., & Marshall, P. J., 2013b, ApJ, 777, 97.
- Sonnenfeld, A., et al., 2015, ApJ, 800, 94.
- Strauss, M. A., et al., 2002, AJ, 124, 1810.
- Suyu, S. H., et al., 2017, MNRAS, 468, 2590.
- Treu, T. & Koopmans, L. V. E., 2002, ApJ, 575, 87.
- Treu, T. & Koopmans, L. V. E., 2004, ApJ, 611, 739.
- Treu, T., & Marshall, P. J., 2016, A&Arv, 24, 11.
- Treu, T, et al., 2018, MNRAS, 481, 1041.
- Turner, E. L., Ostriker, J. P., & Gott, J. R., III, 1984, ApJ, 284, 1.
- Wambsganss, J., 1998, Living Reviews in Relativity, 1, 12.
- Wang, N. & Xu, L., 2013, MPLA, 28, 1350057.
- Wei, J.-J. & Wu, X.-F., 2017, MNRAS 472, 2906.
- Wen, S., Wang, S., & Luo, X., JCAP, 07, 011.
- Xia, J.-Q., et al., 2017, ApJ, 834, 75.
- Xu, D., et al., 2017, MNRAS, 469, 1824.

Table 1: Observational data of the selected galaxy-scale SGL systems

Lens Name	z_l	z_s	θ_E ["]	θ_{eff} ["]	slit["×"]	Fiber radius ["]	θ_{ap} ["]	σ_{ap} [km/s]	Survey Name
MG2016+112	1.004	3.263	1.56	0.31	1.0×1.25	...	0.65	304 ± 27	LSD
0047-281	0.485	3.595	1.34	0.82	0.4×1.25	...	0.41	219 ± 12	LSD
CFRS03.1077	0.938	2.941	1.24	1.60	0.5×1.25	...	0.46	256 ± 19	LSD
HST14176+5226	0.810	3.399	1.41	1.06	0.32×1.25	...	0.37	212 ± 18	LSD
HSTT15433+5352	0.497	2.092	0.36	0.41	0.3×1.25	...	0.35	108 ± 14	LSD
SL2SJ0205-9302	0.557	1.330	0.76	0.75	0.9×1.60	...	0.69	276 ± 37	SL2S
SL2SJ0212-0555	0.750	2.740	1.27	1.22	0.9×1.60	...	0.69	273 ± 22	SL2S
SL2SJ0213-0743	0.717	3.480	2.39	1.97	1.0×1.68	...	0.75	293 ± 34	SL2S
SL2SJ0214-0405	0.609	1.880	1.41	1.21	1.0×1.88	...	0.79	287 ± 47	SL2S
SL2SJ0217-0513	0.646	1.850	1.27	0.73	1.5×1.68	...	0.92	239 ± 27	SL2S
SL2SJ0218-0802	0.884	2.060	1.00	1.02	0.9×1.60	...	0.69	246 ± 48	SL2S
SL2SJ02192-0829	0.389	2.150	1.30	0.95	1.0×1.68	...	0.75	289 ± 23	SL2S
SL2SJ0220-0949	0.572	2.610	1.00	0.53	1.0×1.90	...	0.80	254 ± 29	SL2S
SL2SJ0225-0454	0.238	1.200	1.76	2.12	1.0×0.81	...	0.52	234 ± 21	SL2S
SL2SJ0226-0420	0.494	1.230	1.19	0.84	1.0×1.62	...	0.74	263 ± 24	SL2S
SL2SJ0232-0408	0.352	2.340	1.04	1.14	1.0×1.68	...	0.75	281 ± 26	SL2S
SL2SJ0848-0351	0.682	1.550	0.85	0.45	0.9×1.60	...	0.69	197 ± 21	SL2S
SL2SJ0849-0412	0.722	1.540	1.10	0.46	0.9×1.60	...	0.69	320 ± 24	SL2S
SL2SJ0849-0251	0.274	2.090	1.16	1.34	0.9×1.60	...	0.69	276 ± 35	SL2S
SL2SJ0855-0147	0.365	3.390	1.03	0.69	0.7×1.62	...	0.62	222 ± 25	SL2S
SL2SJ0904-0059	0.611	2.360	1.40	2.00	0.9×1.60	...	0.69	183 ± 21	SL2S
SL2SJ0959+0206	0.552	3.350	0.74	0.46	0.9×1.60	...	0.69	188 ± 22	SL2S
SL2SJ1359+5535	0.783	2.770	1.14	1.13	1.0×1.62	...	0.74	228 ± 29	SL2S
SL2SJ1404+5200	0.456	1.590	2.55	2.03	1.0×1.62	...	0.74	342 ± 20	SL2S
SL2SJ1405+5243	0.526	3.010	1.51	0.83	1.0×1.62	...	0.74	284 ± 21	SL2S
SL2SJ1406+5226	0.716	1.470	0.94	0.80	1.0×1.62	...	0.74	253 ± 19	SL2S
SL2SJ1411+5651	0.322	1.420	0.93	0.85	1.0×1.62	...	0.74	214 ± 23	SL2S
SL2SJ1420+5630	0.483	3.120	1.40	1.62	1.0×1.62	...	0.74	228 ± 19	SL2S
SL2SJ2203+0205	0.400	2.150	1.95	0.99	1.0×1.62	...	0.74	213 ± 21	SL2S
SL2SJ2205+0147	0.476	2.530	1.66	0.66	0.9×1.60	...	0.69	317 ± 30	SL2S
SL2SJ2221+0115	0.325	2.350	1.40	1.12	1.0×1.88	...	0.79	222 ± 23	SL2S
SDSSJ0037-0942	0.195	0.632	1.53	2.30	...	1.5	1.5	279 ± 10	SLACS
SDSSJ0044+0113	0.120	0.197	0.80	2.83	...	1.5	1.5	266 ± 13	SLACS
SDSSJ0216-0813	0.332	0.523	1.16	2.76	...	1.5	1.5	333 ± 23	SLACS
SDSSJ0252+0039	0.280	0.982	1.04	1.34	...	1.5	1.5	164 ± 12	SLACS
SDSSJ0330-0020	0.351	1.071	1.10	1.26	...	1.5	1.5	212 ± 21	SLACS
SDSSJ0728+3835	0.206	0.688	1.25	1.74	...	1.5	1.5	214 ± 11	SLACS
SDSSJ0822+2652	0.241	0.594	1.17	2.01	...	1.5	1.5	259 ± 15	SLACS
SDSSJ0912+0029	0.164	0.324	1.63	4.15	...	1.5	1.5	326 ± 12	SLACS
SDSSJ0936+0913	0.190	0.588	1.09	2.21	...	1.5	1.5	243 ± 11	SLACS
SDSSJ0946+1006	0.222	0.609	1.38	2.54	...	1.5	1.5	263 ± 21	SLACS
SDSSJ0956+5100	0.241	0.470	1.33	2.25	...	1.5	1.5	334 ± 15	SLACS
SDSSJ0959+0410	0.126	0.535	0.99	1.48	...	1.5	1.5	197 ± 13	SLACS
SDSSJ0959+4416	0.237	0.531	0.96	1.93	...	1.5	1.5	244 ± 19	SLACS
SDSSJ1016+3859	0.168	0.439	1.09	1.53	...	1.5	1.5	247 ± 13	SLACS
SDSSJ1020+1122	0.282	0.553	1.20	1.46	...	1.5	1.5	282 ± 18	SLACS
SDSSJ1023+4230	0.191	0.696	1.41	1.88	...	1.5	1.5	242 ± 15	SLACS
SDSSJ1029+0420	0.104	0.615	1.01	1.58	...	1.5	1.5	210 ± 9	SLACS
SDSSJ1106+5228	0.095	0.407	1.23	2.05	...	1.5	1.5	262 ± 9	SLACS
SDSSJ1112+0826	0.273	0.629	1.49	1.55	...	1.5	1.5	320 ± 20	SLACS
SDSSJ1134+6027	0.153	0.474	1.10	1.98	...	1.5	1.5	239 ± 11	SLACS
SDSSJ1142+1001	0.222	0.504	0.98	1.95	...	1.5	1.5	221 ± 22	SLACS
SDSSJ1143-0144	0.106	0.402	1.68	5.28	...	1.5	1.5	269 ± 5	SLACS
SDSSJ1153+4612	0.180	0.875	1.05	1.32	...	1.5	1.5	226 ± 15	SLACS
SDSSJ1204+0358	0.164	0.631	1.31	1.63	...	1.5	1.5	267 ± 17	SLACS
SDSSJ1205+4910	0.215	0.481	1.22	2.59	...	1.5	1.5	281 ± 13	SLACS
SDSSJ1218+0830	0.135	0.717	1.45	3.18	...	1.5	1.5	219 ± 10	SLACS
SDSSJ1250+0523	0.232	0.795	1.13	1.86	...	1.5	1.5	252 ± 14	SLACS

Table 1
(continued)

Lens Name	z_l	z_s	θ_E ["]	θ_{eff} ["]	slit[" \times "]	Fiber radius ["]	θ_{ap} ["]	σ_{ap} [km/s]	Survey Name
SDSSJ1306+0600	0.173	0.472	1.32	2.08	...	1.5	1.5	237 ± 17	SLACS
SDSSJ1313+4615	0.185	0.514	1.37	2.10	...	1.5	1.5	263 ± 18	SLACS
SDSSJ1318-0313	0.240	1.300	1.58	3.70	...	1.5	1.5	213 ± 18	SLACS
SDSSJ1330-0148	0.081	0.711	0.86	0.91	...	1.5	1.5	185 ± 9	SLACS
SDSSJ1402+6321	0.205	0.481	1.35	2.65	...	1.5	1.5	267 ± 17	SLACS
SDSSJ1403+0006	0.189	0.473	0.83	1.62	...	1.5	1.5	213 ± 17	SLACS
SDSSJ1416+5136	0.299	0.811	1.37	1.33	...	1.5	1.5	240 ± 25	SLACS
SDSSJ1420+6019	0.063	0.535	1.04	2.11	...	1.5	1.5	205 ± 4	SLACS
SDSSJ1430+4105	0.285	0.575	1.52	2.42	...	1.5	1.5	322 ± 32	SLACS
SDSSJ1436-0000	0.285	0.805	1.12	2.41	...	1.5	1.5	224 ± 17	SLACS
SDSSJ1443+0304	0.134	0.419	0.81	1.11	...	1.5	1.5	209 ± 11	SLACS
SDSSJ1451-0239	0.125	0.520	1.04	2.60	...	1.5	1.5	223 ± 14	SLACS
SDSSJ1525+3327	0.358	0.717	1.31	2.82	...	1.5	1.5	264 ± 26	SLACS
SDSSJ1531-0105	0.160	0.744	1.71	2.73	...	1.5	1.5	279 ± 12	SLACS
SDSSJ1538+5817	0.143	0.531	1.00	1.45	...	1.5	1.5	189 ± 12	SLACS
SDSSJ1621+3931	0.245	0.602	1.29	2.30	...	1.5	1.5	236 ± 20	SLACS
SDSSJ1627-0053	0.208	0.524	1.23	2.02	...	1.5	1.5	290 ± 14	SLACS
SDSSJ1630+4520	0.248	0.793	1.78	2.01	...	1.5	1.5	276 ± 16	SLACS
SDSSJ1636+4707	0.228	0.675	1.08	1.62	...	1.5	1.5	231 ± 15	SLACS
SDSSJ1644+2625	0.137	0.610	1.27	1.85	...	1.5	1.5	229 ± 12	SLACS
SDSSJ1719+2939	0.181	0.578	1.28	1.42	...	1.5	1.5	286 ± 15	SLACS
SDSSJ2238-0754	0.137	0.713	1.27	2.39	...	1.5	1.5	198 ± 11	SLACS
SDSSJ2300+0022	0.228	0.463	1.24	1.88	...	1.5	1.5	279 ± 17	SLACS
SDSSJ2303+1422	0.155	0.517	1.62	3.46	...	1.5	1.5	255 ± 16	SLACS
SDSSJ2321-0939	0.082	0.532	1.60	4.22	...	1.5	1.5	249 ± 8	SLACS
SDSSJ2341+0000	0.186	0.807	1.44	3.40	...	1.5	1.5	207 ± 13	SLACS
SDSSJ0143-1006	0.221	1.105	1.23	2.18	...	1.5	1.5	216 ± 15	S4TM
SDSSJ0159-0006	0.158	0.748	0.92	0.67	...	1.5	1.5	233 ± 13	S4TM
SDSSJ0324-0110	0.446	0.624	0.63	1.21	...	1.5	1.5	235 ± 26	S4TM
SDSSJ0324+0045	0.321	0.920	0.55	1.24	...	1.5	1.5	145 ± 18	S4TM
SDSSJ0753+3416	0.137	0.963	1.24	1.84	...	1.5	1.5	202 ± 9	S4TM
SDSSJ0754+1927	0.153	0.740	1.05	2.71	...	1.5	1.5	187 ± 12	S4TM
SDSSJ0757+1956	0.121	0.833	1.92	1.52	...	1.5	1.5	234 ± 9	S4TM
SDSSJ0826+5630	0.132	1.291	1.02	1.75	...	1.5	1.5	151 ± 6	S4TM
SDSSJ0847+2348	0.155	0.533	0.96	1.34	...	1.5	1.5	200 ± 12	S4TM
SDSSJ0851+0505	0.128	0.637	0.90	1.27	...	1.5	1.5	175 ± 9	S4TM
SDSSJ0920+3028	0.288	0.392	0.70	1.72	...	1.5	1.5	308 ± 13	S4TM
SDSSJ0955+3014	0.321	0.467	0.53	2.07	...	1.5	1.5	273 ± 23	S4TM
SDSSJ0956+5539	0.196	0.848	1.17	2.41	...	1.5	1.5	196 ± 8	S4TM
SDSSJ1010+3124	0.167	0.425	1.13	2.96	...	1.5	1.5	235 ± 9	S4TM
SDSSJ1041+0112	0.101	0.217	0.60	2.13	...	1.5	1.5	197 ± 6	S4TM
SDSSJ1048+1313	0.133	0.668	1.20	2.97	...	1.5	1.5	202 ± 7	S4TM
SDSSJ1051+4439	0.163	0.538	0.99	2.73	...	1.5	1.5	208 ± 12	S4TM
SDSSJ1056+4141	0.134	0.832	0.73	1.10	...	1.5	1.5	145 ± 8	S4TM
SDSSJ1101+1523	0.178	0.517	1.18	0.74	...	1.5	1.5	295 ± 12	S4TM
SDSSJ1116+0729	0.170	0.686	0.82	4.72	...	1.5	1.5	177 ± 9	S4TM
SDSSJ1127+2312	0.130	0.361	1.26	4.49	...	1.5	1.5	244 ± 7	S4TM
SDSSJ1137+1818	0.124	0.463	1.29	1.57	...	1.5	1.5	223 ± 6	S4TM
SDSSJ1142+2509	0.164	0.659	0.79	1.60	...	1.5	1.5	158 ± 7	S4TM
SDSSJ1144+0436	0.104	0.255	0.76	1.75	...	1.5	1.5	240 ± 12	S4TM
SDSSJ1213+2930	0.091	0.595	1.35	1.92	...	1.5	1.5	236 ± 6	S4TM
SDSSJ1301+0834	0.090	0.533	1.00	4.74	...	1.5	1.5	185 ± 6	S4TM
SDSSJ1330+1750	0.207	0.372	1.02	1.90	...	1.5	1.5	263 ± 9	S4TM
SDSSJ1403+3309	0.062	0.772	1.03	3.55	...	1.5	1.5	207 ± 5	S4TM
SDSSJ1430+6104	0.169	0.654	1.00	5.87	...	1.5	1.5	203 ± 13	S4TM
SDSSJ1433+2835	0.091	0.411	1.53	2.70	...	1.5	1.5	238 ± 5	S4TM
SDSSJ1541+3642	0.141	0.739	1.15	1.41	...	1.5	1.5	183 ± 8	S4TM
SDSSJ1543+2202	0.268	0.397	0.78	1.71	...	1.5	1.5	294 ± 14	S4TM

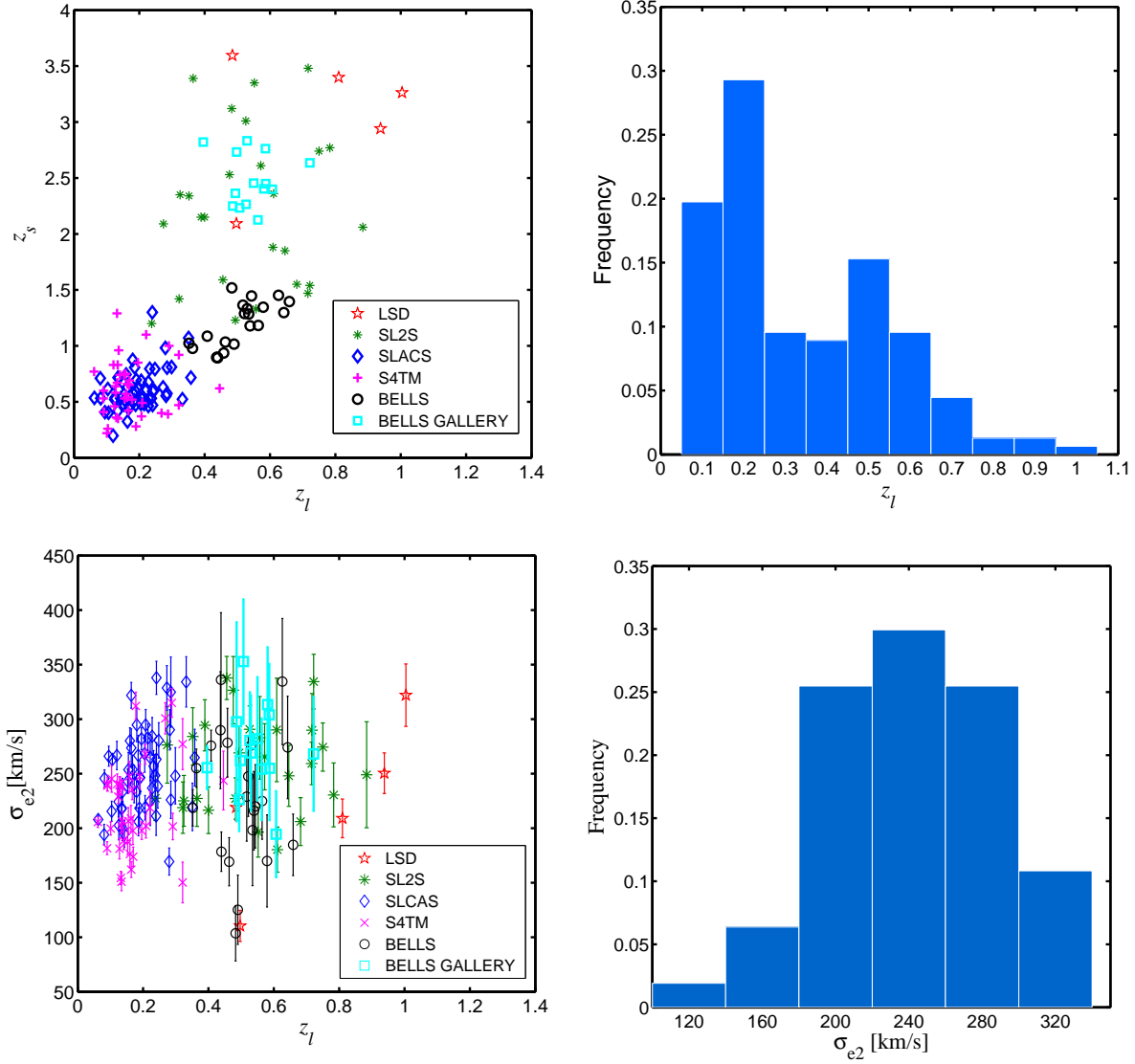
Table 1
(continued)

Lens Name	z_l	z_s	θ_E ["]	θ_{eff} ["]	slit["×"]	Fiber radius ["]	θ_{ap} ["]	σ_{ap} [km/s]	Survey Name
SDSSJ1550+2020	0.135	0.350	1.01	2.34	...	1.5	1.5	235 ± 7	S4TM
SDSSJ1553+3004	0.160	0.566	0.84	7.62	...	1.5	1.5	183 ± 13	S4TM
SDSSJ1607+2147	0.209	0.487	0.56	2.63	...	1.5	1.5	201 ± 11	S4TM
SDSSJ1633+1441	0.128	0.580	1.39	3.19	...	1.5	1.5	240 ± 8	S4TM
SDSSJ2309-0039	0.291	1.005	1.14	2.19	...	1.5	1.5	199 ± 12	S4TM
SDSSJ2324+0105	0.190	0.278	0.59	1.27	...	1.5	1.5	239 ± 11	S4TM
SDSSJ0801+4727	0.483	1.518	0.49	0.50	...	1	1	98 ± 24	BELLS
SDSSJ1234-0241	0.490	1.016	0.53	1.05	...	1	1	122 ± 31	BELLS
SDSSJ1352+3216	0.463	1.034	1.82	0.58	...	1	1	161 ± 21	BELLS
SDSSJ1159-0007	0.579	1.346	0.68	0.96	...	1	1	165 ± 41	BELLS
SDSSJ1318-0104	0.659	1.396	0.68	0.69	...	1	1	177 ± 27	BELLS
SDSSJ1349+3612	0.440	0.893	0.75	1.89	...	1	1	178 ± 18	BELLS
SDSSJ1221+3806	0.535	1.284	0.70	0.47	...	1	1	187 ± 48	BELLS
SDSSJ0944-0147	0.539	1.179	0.73	0.48	...	1	1	204 ± 34	BELLS
SDSSJ1601+2138	0.544	1.446	0.86	0.44	...	1	1	207 ± 36	BELLS
SDSSJ1542+1629	0.352	1.023	1.04	0.73	...	1	1	210 ± 16	BELLS
SDSSJ0151+0049	0.517	1.364	0.68	0.67	...	1	1	219 ± 39	BELLS
SDSSJ1337+3620	0.564	1.182	1.39	2.03	...	1	1	225 ± 35	BELLS
SDSSJ2125+0411	0.363	0.978	1.20	0.90	...	1	1	247 ± 17	BELLS
SDSSJ1545+2748	0.522	1.289	1.21	2.59	...	1	1	250 ± 37	BELLS
SDSSJ1215+0047	0.642	1.297	1.37	0.65	...	1	1	262 ± 45	BELLS
SDSSJ0830+5116	0.530	1.332	1.14	0.97	...	1	1	268 ± 36	BELLS
SDSSJ1631+1854	0.408	1.086	1.63	1.43	...	1	1	272 ± 14	BELLS
SDSSJ2303+0037	0.458	0.936	1.02	1.35	...	1	1	274 ± 31	BELLS
SDSSJ0747+4448	0.437	0.897	0.61	0.92	...	1	1	281 ± 52	BELLS
SDSSJ2122+0409	0.626	1.452	1.58	0.90	...	1	1	324 ± 56	BELLS
SDSSJ0747+5055	0.438	0.898	0.75	1.09	...	1	1	328 ± 60	BELLS
SDSSJ0201+3228	0.396	2.821	1.70	2.32	...	1	1	257 ± 20	BELLS GALLERY
SDSSJ0237-0641	0.486	2.249	0.65	1.05	...	1	1	290 ± 89	BELLS GALLERY
SDSSJ0742+3341	0.494	2.363	1.22	0.89	...	1	1	219 ± 28	BELLS GALLERY
SDSSJ1226+5457	0.498	2.732	1.37	0.56	...	1	1	249 ± 27	BELLS GALLERY
SDSSJ0856+2010	0.507	2.233	0.98	0.51	...	1	1	334 ± 54	BELLS GALLERY
SDSSJ2342-0120	0.527	2.265	1.11	1.75	...	1	1	279 ± 44	BELLS GALLERY
SDSSJ2228+1205	0.530	2.832	1.28	0.53	...	1	1	255 ± 50	BELLS GALLERY
SDSSJ1116+0915	0.550	2.454	1.03	0.98	...	1	1	274 ± 55	BELLS GALLERY
SDSSJ1201+4743	0.563	2.126	1.18	0.48	...	1	1	240 ± 44	BELLS GALLERY
SDSSJ0918+5104	0.581	2.403	1.60	0.57	...	1	1	298 ± 50	BELLS GALLERY
SDSSJ1141+2216	0.586	2.762	1.27	0.44	...	1	1	286 ± 44	BELLS GALLERY
SDSSJ0029+2544	0.587	2.450	1.34	0.49	...	1	1	241 ± 45	BELLS GALLERY
SDSSJ1110+2808	0.607	2.400	0.98	1.45	...	1	1	192 ± 39	BELLS GALLERY
SDSSJ0755+3445	0.722	2.635	2.05	2.89	...	1	1	272 ± 53	BELLS GALLERY

NOTE – The columns are: (1) Lens name;(2) lens redshift;(3) source redshift;(4) Einstein angle;(5) effective radius;(6) angular sizes of width and length of the rectangular aperture; (7) angular radius of the fiber;(8) angular radius of the circular aperture, for the rectangular aperture the corresponding equivalent value derived with Eq. (18); (9) velocity dispersion measured inside the circular aperture with the angular radius θ_{ap} ;(10) survey name.

Table 2. Observational constraints on three lens mass models with our lens sample. We present the mean values with 68% confidence limits for the model parameters.

Lens Model			Parameters		
Model 1	$\gamma = 1.981^{+0.024}_{-0.023}$	$\delta = 2.008^{+0.499}_{-0.563}$	$\beta = -0.388^{+0.670}_{-0.344}$
Model 2	$\gamma_0 = 2.070^{+0.031}_{-0.028}$	$\gamma_z = -0.119^{+0.050}_{-0.064}$...	$\delta = 2.540^{+0.200}_{-0.296}$	$\beta = -0.357^{+0.398}_{-0.464}$
Model 3	$\gamma_0 = 1.588^{+0.071}_{-0.069}$	$\gamma_z = -0.128^{+0.033}_{-0.039}$	$\gamma_s = 0.349^{+0.055}_{-0.056}$	$\delta = 2.524^{+0.098}_{-0.105}$	$\beta = 0.447^{+0.204}_{-0.224}$

**Figure 1.** The distributions of the lens redshifts z_l , the source redshifts z_s and the lens stellar velocity dispersions σ_{e2} for the SGL sample presented in Table 1. The left panels show the sample distribution in $z_l - z_s$ and $z_l - \sigma_{e2}$ planes, where the points with different colors denote samples from different surveys. The right panels display the normalized histograms of z_l and σ_{e2} for the whole sample.

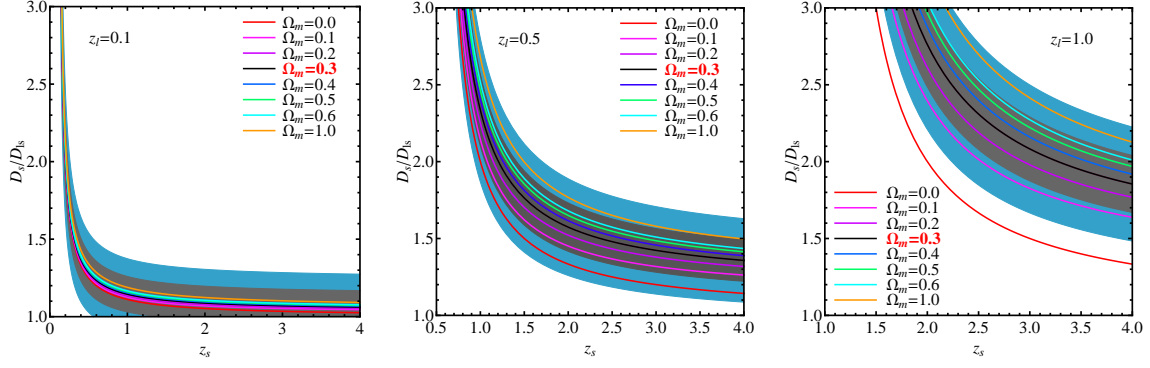


Figure 2. The evolution of the distance ratio D_s/D_{ls} with respect to source redshift z_s with the variety of Ω_m , corresponding to lens redshift $z_l = 0.1, 0.5$ and 1 , where the other cosmological parameters take the fiducial values. In each panel, the solid black line corresponds to the fiducial value of D_s/D_{ls} , which is plotted with the fiducial values of cosmological parameters, and the shadows denote the cases that the relative uncertainties of D_s/D_{ls} are 10% and 20% with respect to the fiducial value.

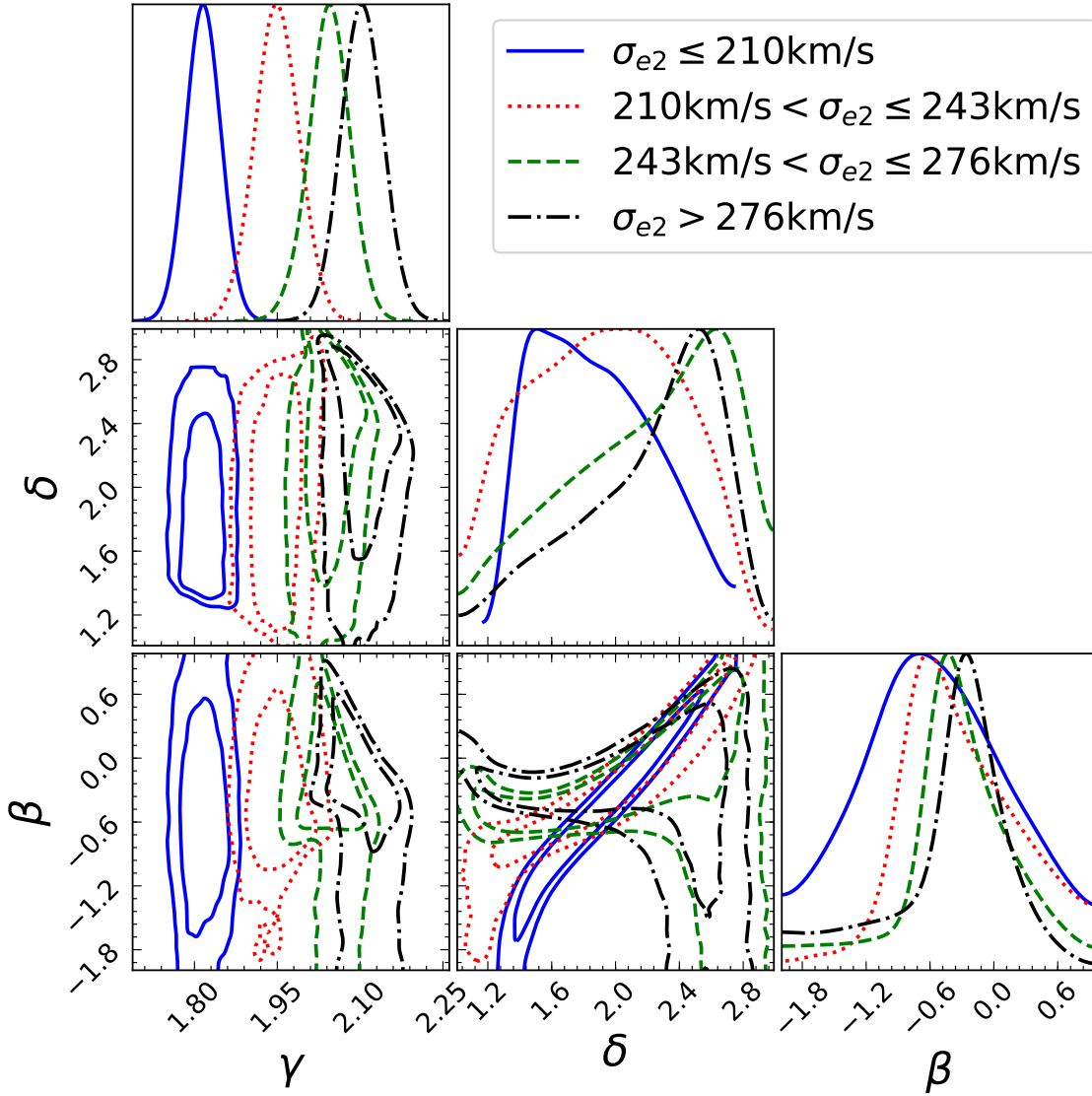


Figure 3. Constraining the lens mass model parameters from four sub-samples defined by different velocity dispersion bins. The 1D probability distributions denote the marginalized likelihoods. And, the 2D contours correspond to 68% and 95% confidence levels.

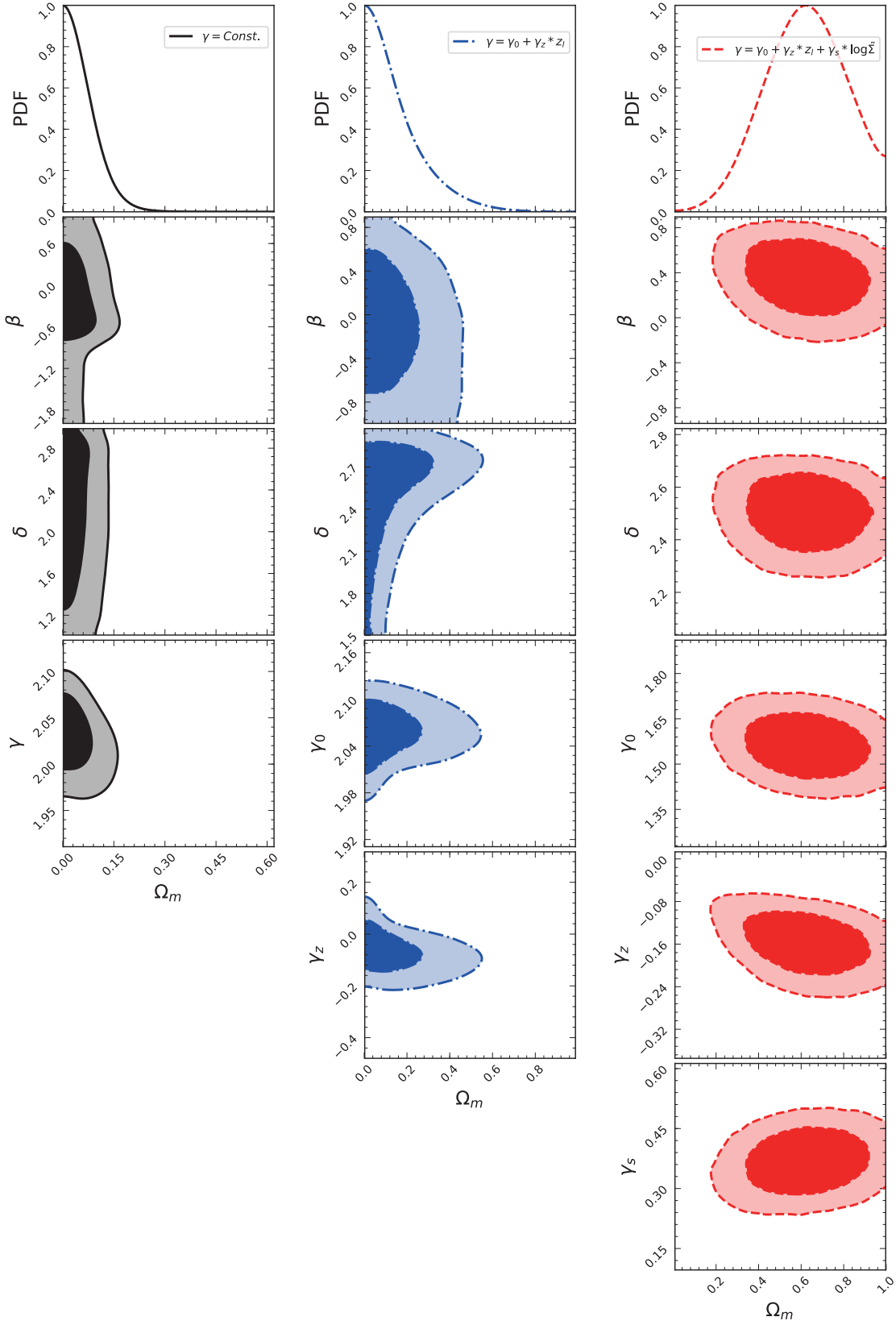


Figure 4. Observational constraints on Ω_m and parameters of lens mass models. The columns, from left to right, correspond to the scenarios with $\gamma = \text{Constant}$, $\gamma = \gamma_0 + \gamma_z * z_l$ and $\gamma = \gamma_0 + \gamma_z * z_l + \gamma_s \log \tilde{\Sigma}$, respectively.

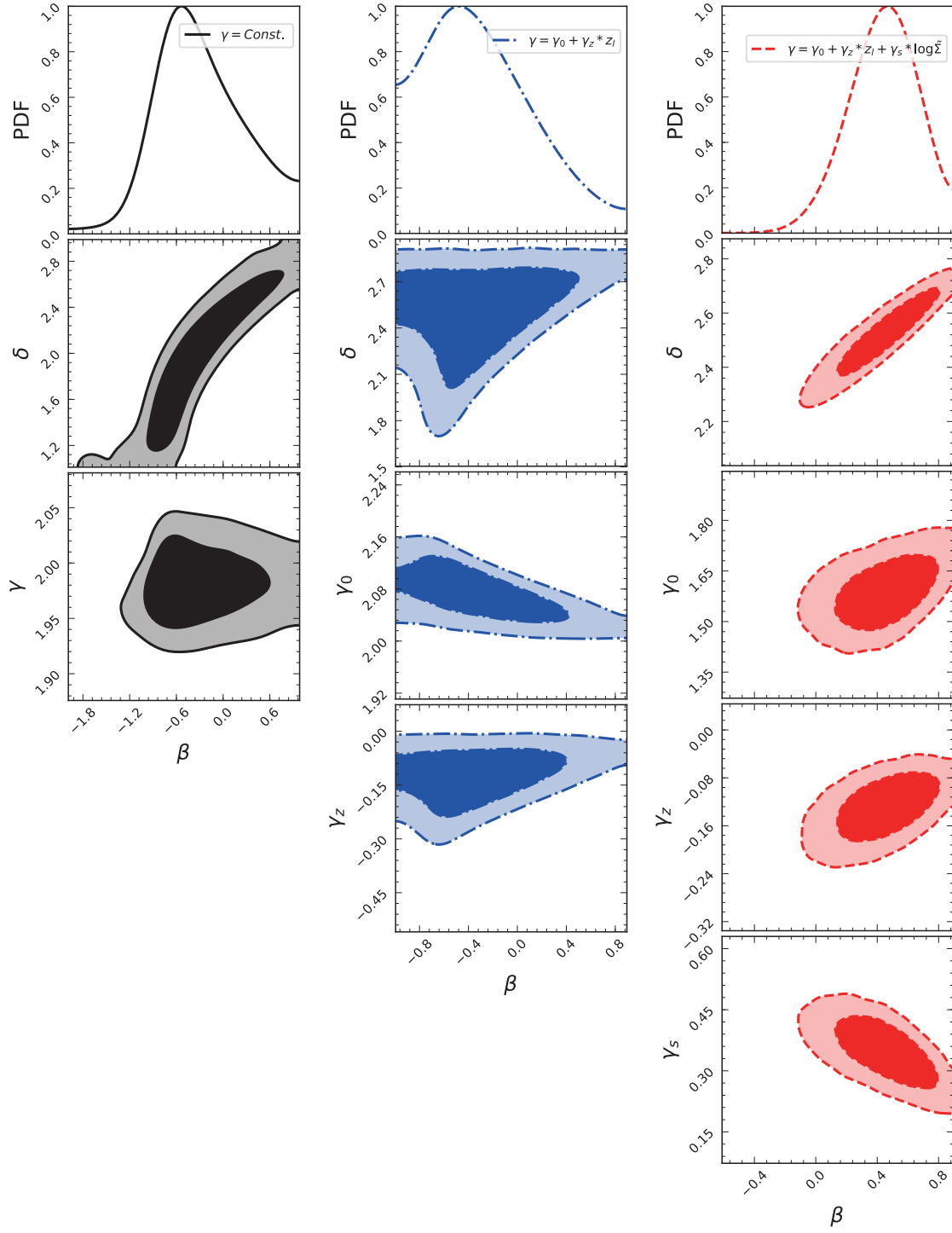


Figure 5. Constraining the lens mass model parameters with the cosmological parameters fixed. The columns, from left to right, correspond to the scenarios with $\gamma = \text{Constant}$, $\gamma = \gamma_0 + \gamma_z * z_l$ and $\gamma = \gamma_0 + \gamma_z * z_l + \gamma_s \log \tilde{\Sigma}$, respectively.